Supporting Information

Rational design of high concentration electrolytes and MXene-based sulfur host materials toward high-performance magnesium sulfur batteries

Hao Xu[a,b,c], Dong Zhu[d,e], Wen Zhu[a,b,c], Fengzhan Sun[a,b,c], Jianxin Zou[a,b,c,*], Richard M. Laine[f,*] and Wenjiang Ding[a,b,c]

[a]National Engineering Research Center of Light Alloy Net Forming, School of Materials Science and Engineering, Shanghai Jiao Tong University, Shanghai, 200240, P. R. China

[b]State Key Laboratory of Metal Matrix Composites, School of Materials Science and Engineering, Shanghai Jiao Tong University, Shanghai, 200240, P. R. China

[c]Center of Hydrogen Science, Shanghai Jiao Tong University, Shanghai, 200240, P. R. China

[d]Computer Network Information Center, Chinese Academy of Science, Beijing, 100190, P. R. China

[e]University of Chinese Academy of Science, Beijing, 100049, P. R. China

[f]Department of Materials Science and Engineering, University of Michigan, Ann Arbor, Michigan 48109-2136, United States

[*]Corresponding authors.

E-mail addresses: zoujx@sjtu.edu.cn (J. X. Z), talsdad@umich.edu (R. M. L)

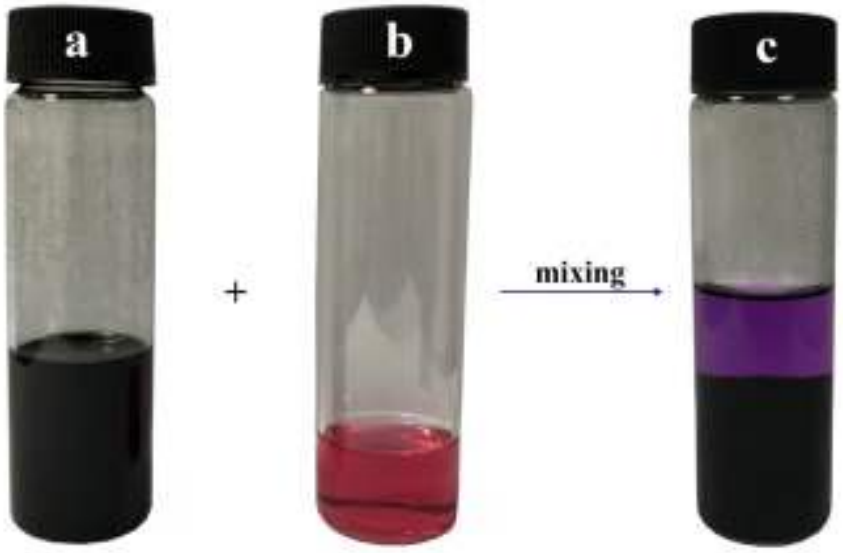

Fig. S1. The preparation process of Ti_3C_2@Co-LDH composites by electrostatic self-assembly. (a) Ti_3C_2 and 2-methylimidazole dispersed in methanol and deionized water. (b) $Co(NO_3)_2 \cdot 6H_2O$ dissolved in methanol. (c) Ti_3C_2@Co-LDH composites precipitating.

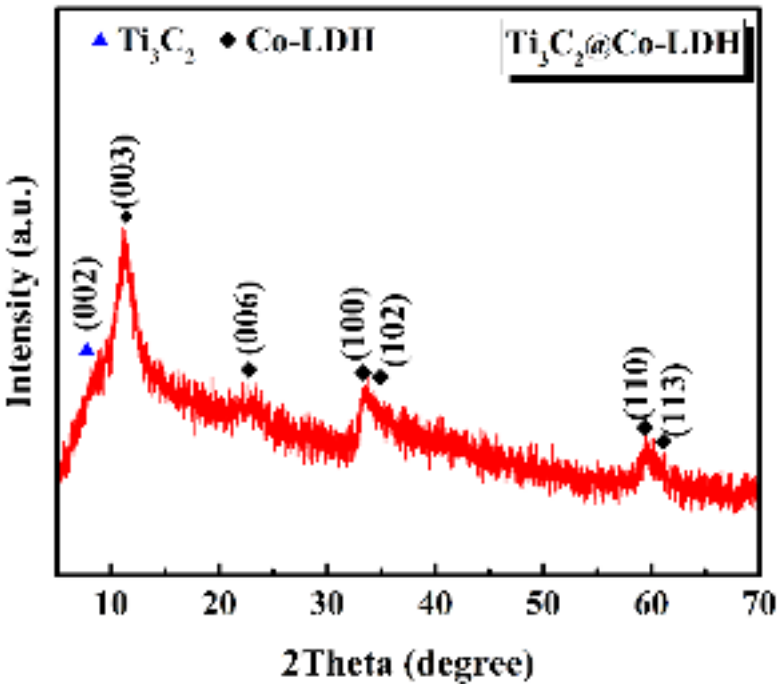

Fig. S2. XRD pattern of Ti_3C_2@Co-LDH composites.

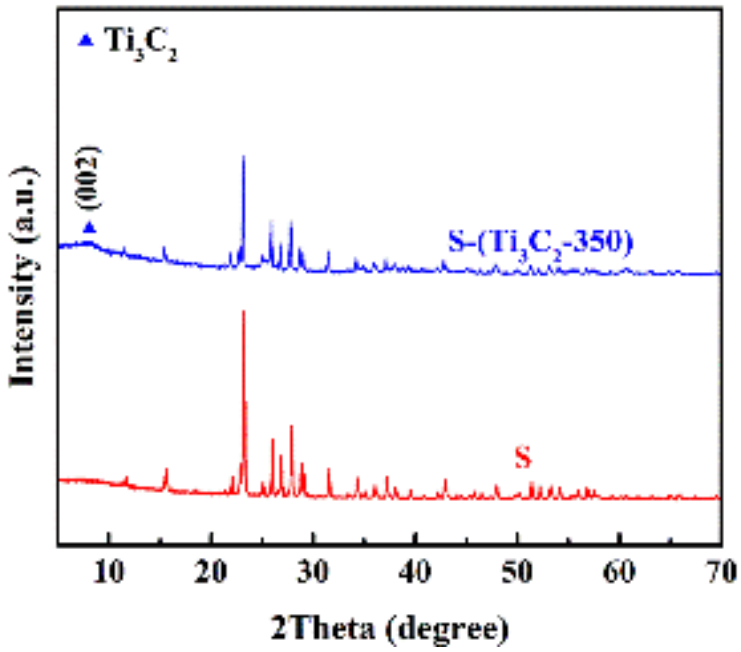

Fig. S3. XRD patterns of S and S-(Ti_3C_2-350) composites.

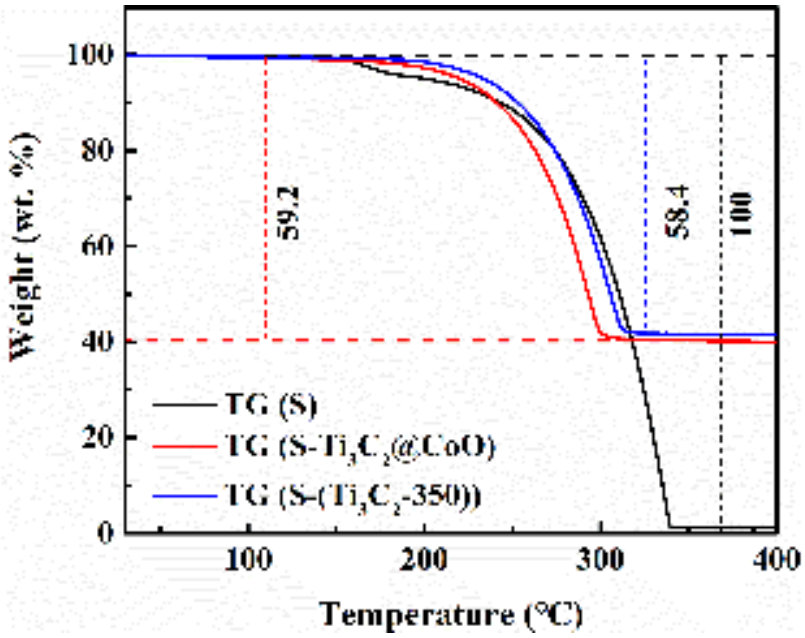

Fig. S4. TG curves of S, S-(Ti_3C_2-350) and S-Ti_3C_2@CoO.

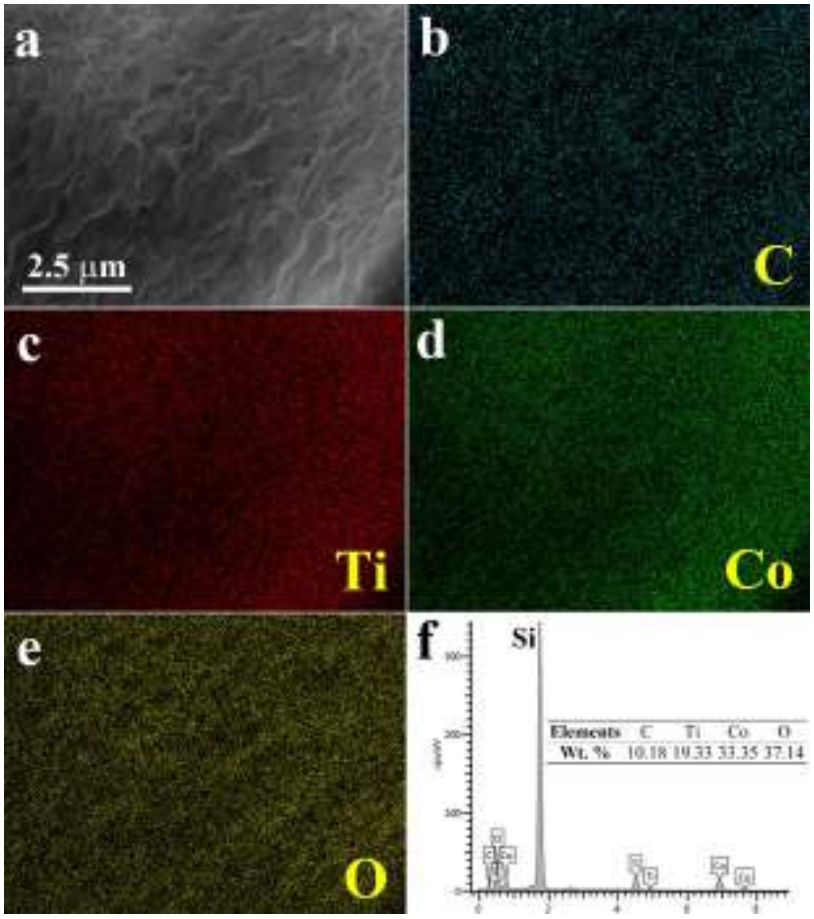

Fig. S5. (a) SEM image and (b-f) EDX results of Ti_3C_2@Co-LDH composites.

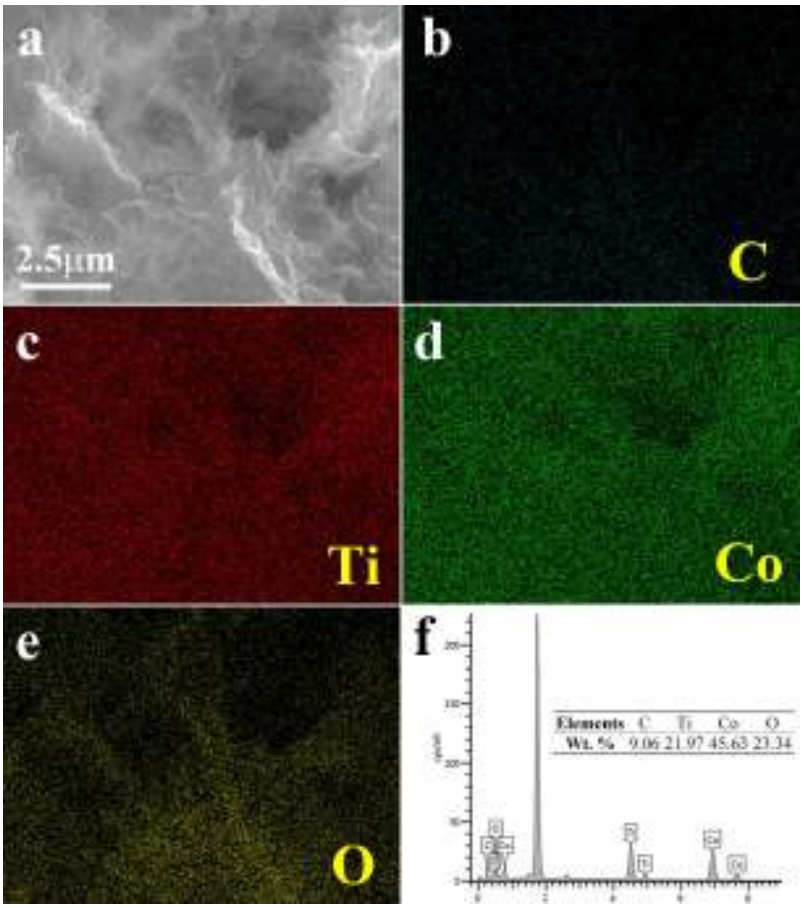

Fig. S6. (a) SEM image and (b-f) EDX results of Ti_3C_2@CoO composites.

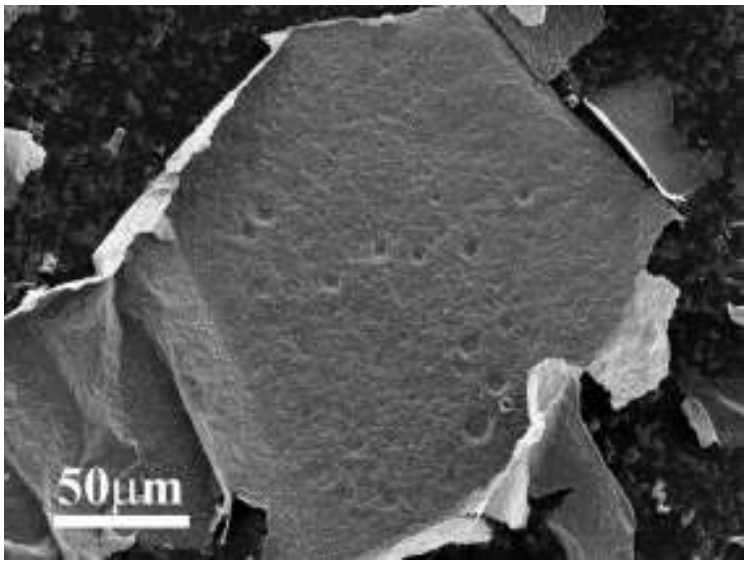

Fig. S7. SEM image of obtained Ti_3C_2 flakes by freeze-drying directly.

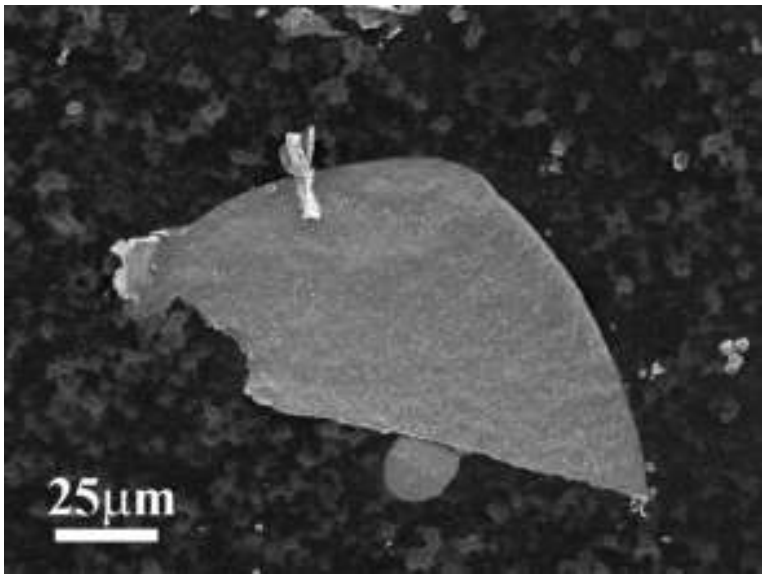

Fig. S8. SEM image of Ti_3C_2-350 flakes after annealing under Ar/H_2 atmosphere at 350℃ for 2h.

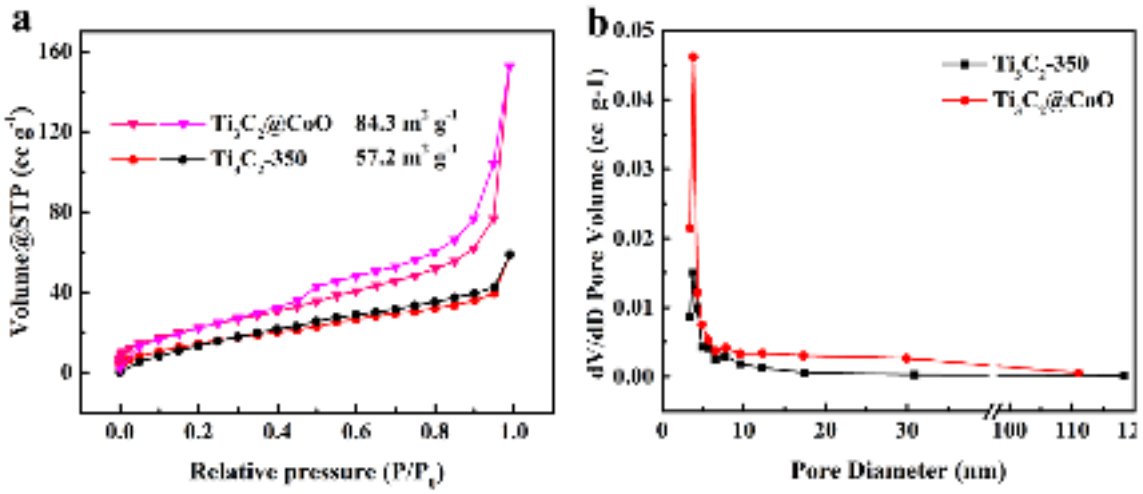

Fig. S9. (a) N_2 adsorption (red, pink) and desorption (black, magenta) isotherms and (b) pore size distribution of Ti_3C_2-350 and Ti_3C_2@CoO.

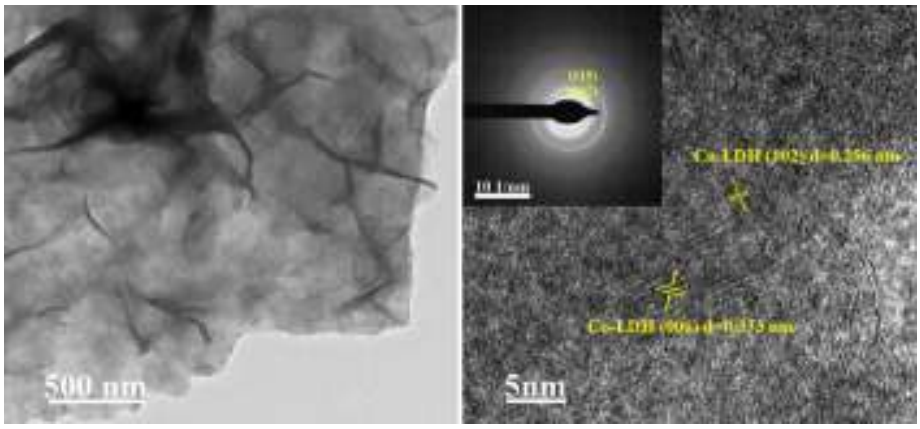

Fig. S10. (a) TEM and (b) HRTEM images of Ti_3C_2@Co-LDH composites and inset is the SAED pattern.

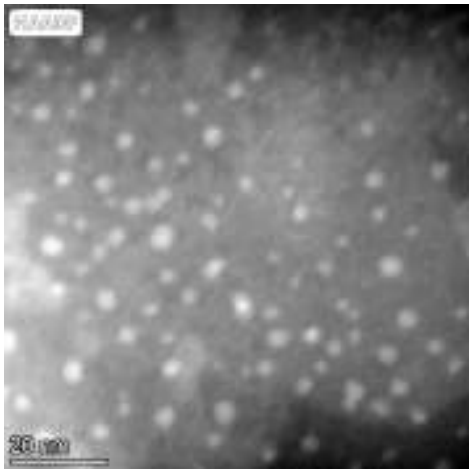

Fig. S11. HAADF image of Ti_3C_2@CoO composite.

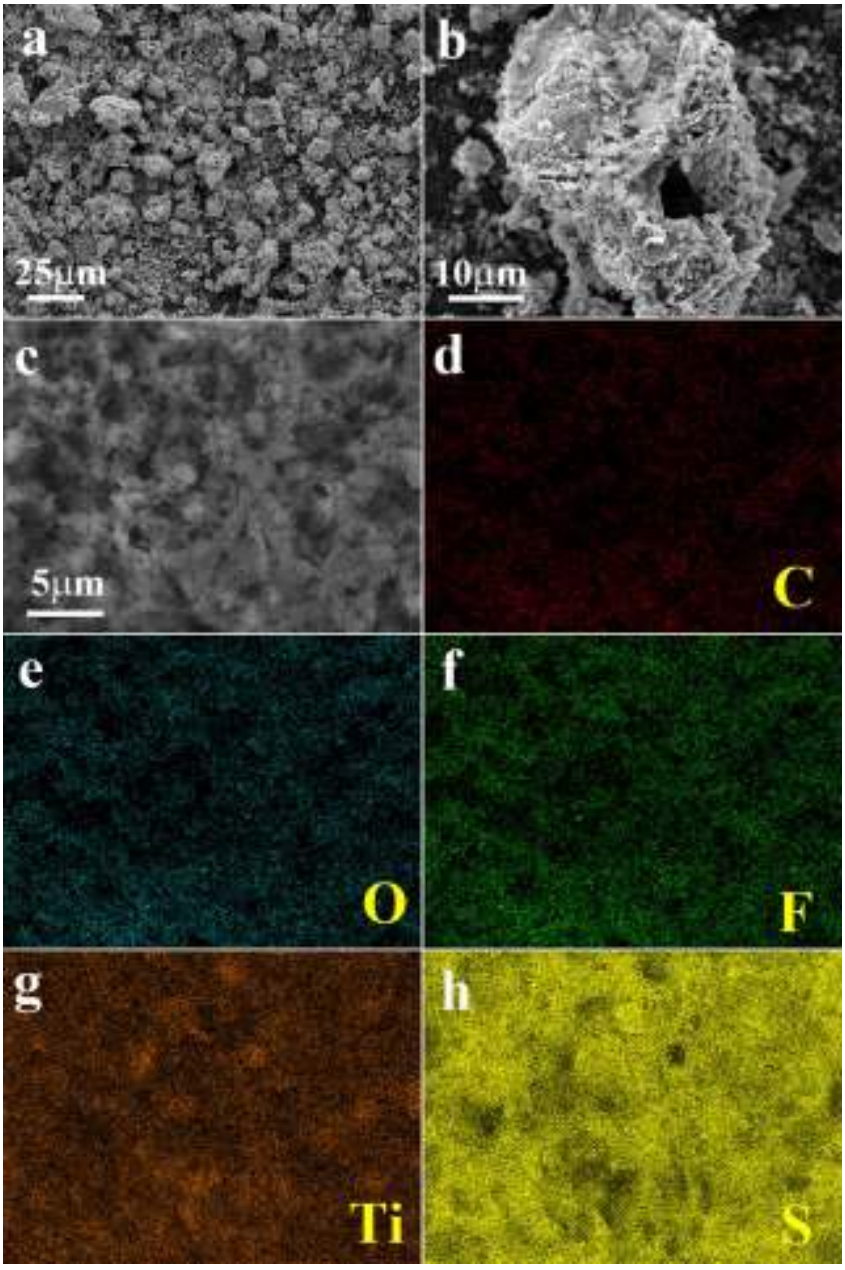

Fig. S12. (a, b) SEM images of S-(Ti_3C_2-350) form different scales and (c-h) EDX results.

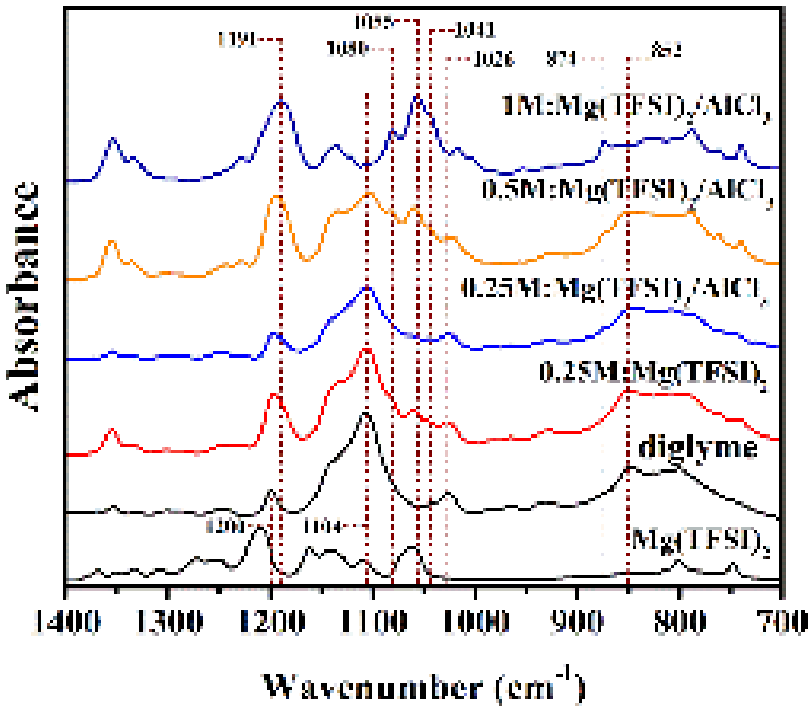

Fig. S13. FT-IR spectra of $Mg(TFSI)_2$, diglyme solvent and 0.25M $Mg(TFSI)_2$, 0.25M $Mg(TFSI)_2$/ $AlCl_3$, 0.5M $Mg(TFSI)_2/AlCl_3$, 1M $Mg(TFSI)_2/AlCl_3$ in diglyme.

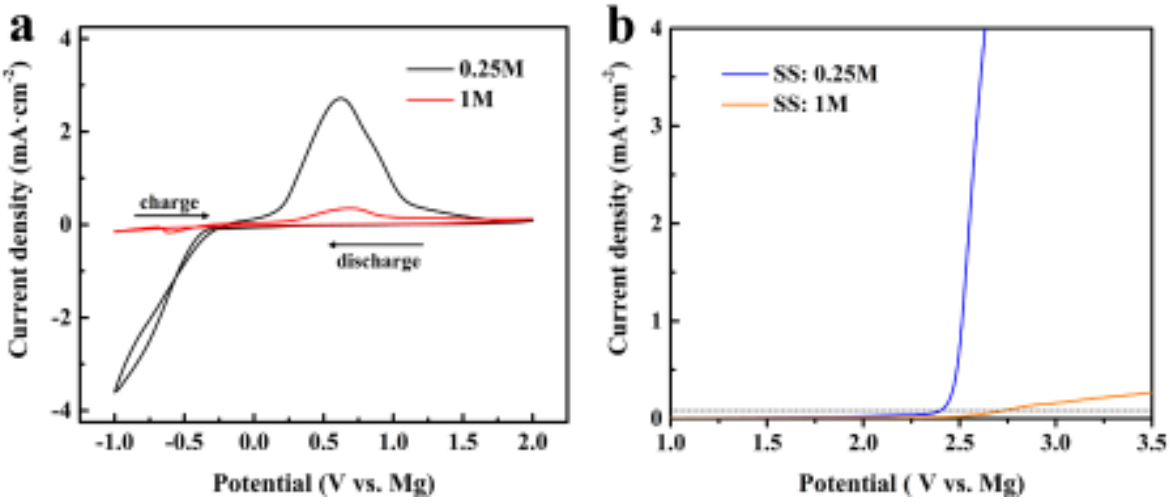

Fig. S14 Electrochemical performance of $Mg(TFSI)_2/AlCl_3$/diglyme electrolytes. (a) CV curves of different electrolytes on SS foils with Mg foils as the counter and reference electrodes. Scan rate: 25 mV s^{-1}. (b) LSV of different electrolytes on SS working electrodes with Mg foils as the counter and reference electrodes. Scan rate: 5 mV s^{-1}.

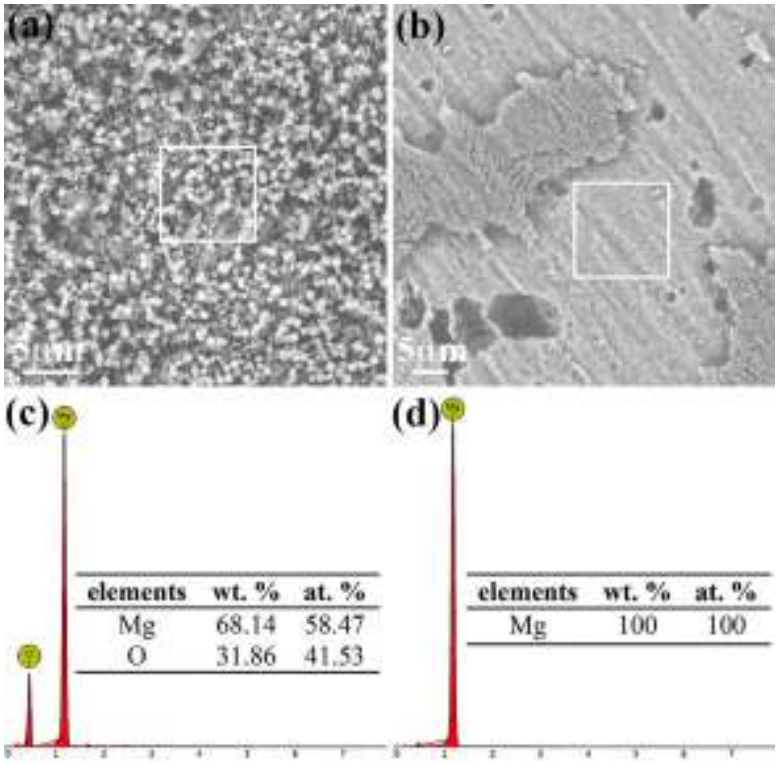

Fig. S15. (a) SEM images and (c) EDX results of deposits on Pt; (b)SEM images and (d)EDX results of Mg anode. The Pt foil with 1 M $Mg(TFSI)_2/AlCl_3$/diglyme electrolyte was applied the potential of 1.2 V vs. Mg (RE) for one hour, where Pt foil was working electrode and Mg foil was counter and reference electrodes.

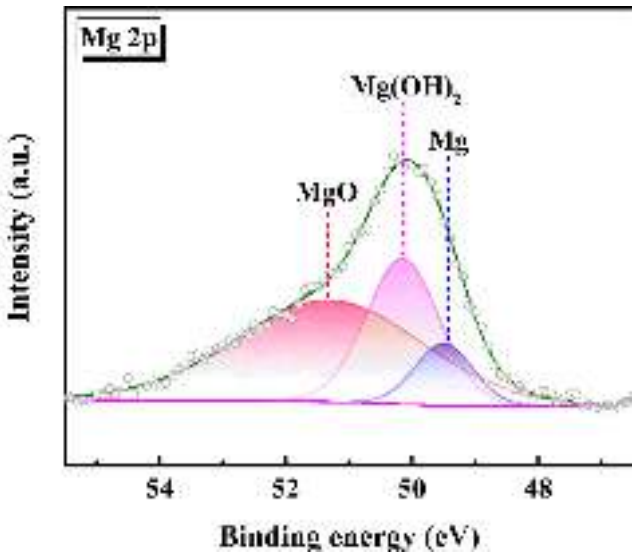

Fig. S16. Mg 2p spectra of deposits on Pt foil.

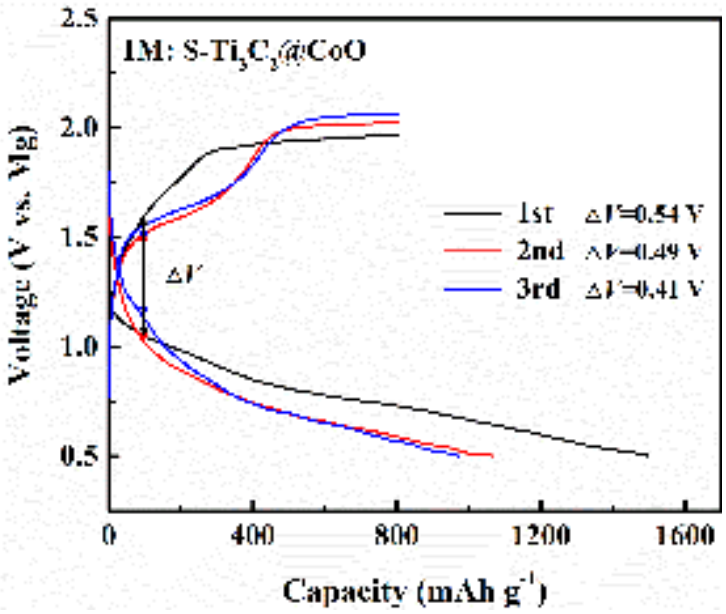

Fig. S17. Discharge and charge profiles of cells using S-Ti_3C_2@CoO electrode and 1 M electrolyte during the 1st, 2nd, 3rd cycles at 100 mA g^{-1}.

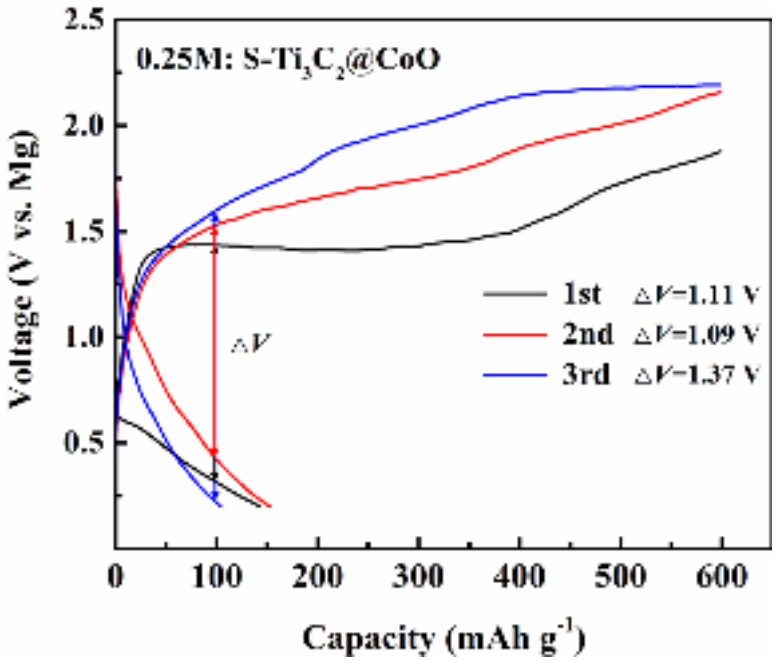

Fig. S18. Discharge and charge profiles of cells using S-Ti_3C_2@CoO electrode and 0.25 M electrolyte during the 1st, 2nd, 3rd cycles at 100 mA g^{-1}

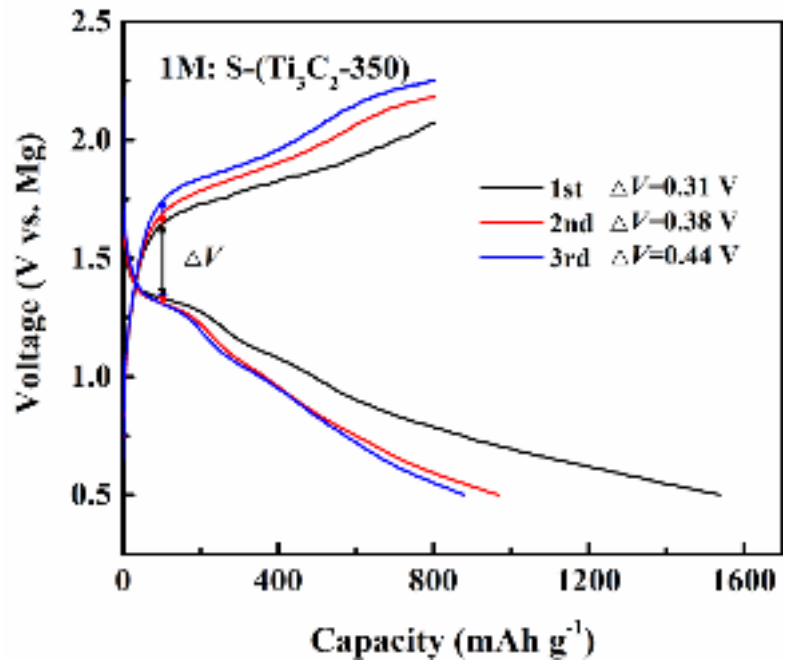

Fig. S19. Discharge and charge profiles of cells using S-(Ti_3C_2-350) electrode and 1 M electrolyte during the 1st, 2nd, 3rd cycles at 100 mA g^{-1}.

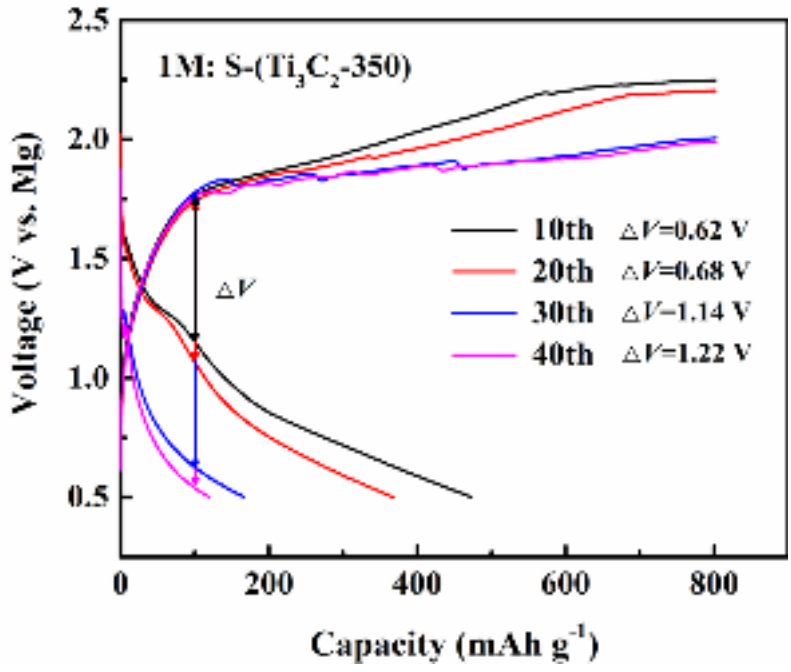

Fig. S20. Charge and discharge profiles of cells using S-(Ti_3C_2-350) electrode and 1 M electrolyte during the 10th , 20th , 30th and 40th cycles at 100 mA g^{-1}.

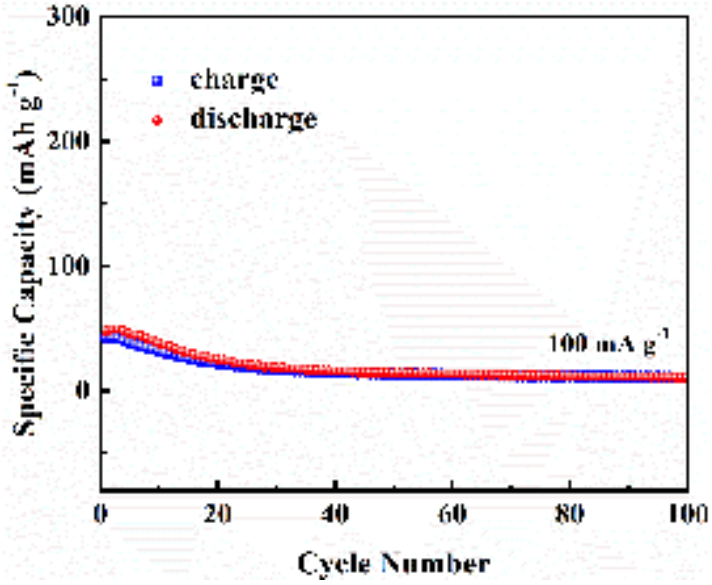

Fig. S21. Cycling performance of MIBs using Ti_3C_2@CoO and 1 M electrolyte at 100 mA g^{-1} for 100 cycles.

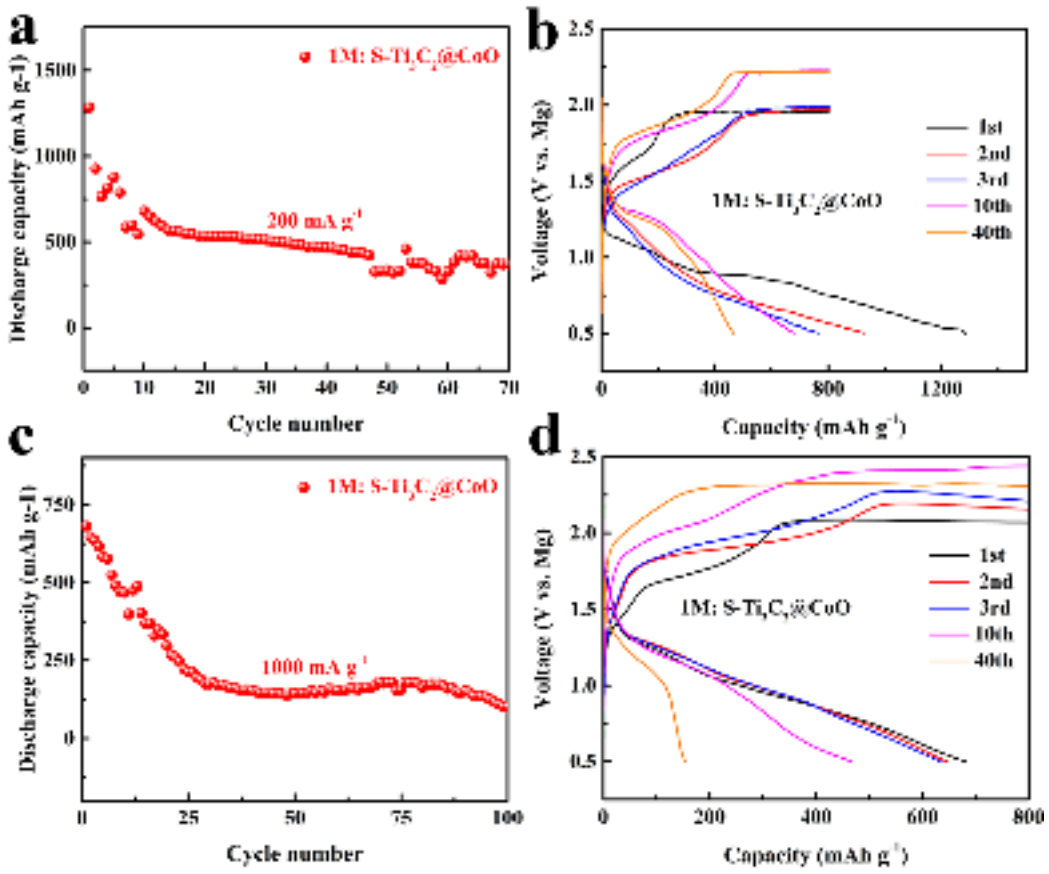

Fig. S22. Cycling performance and corresponding discharge and charge profiles of S- Ti_3C_2@CoO cathodes coupled with 1 M $Mg(TFSI)_2/AlCl_3$/diglyme electrolyte: (a, b) at 200 mA g^{-1} and (c, d) 1000 mA g^{-1}.

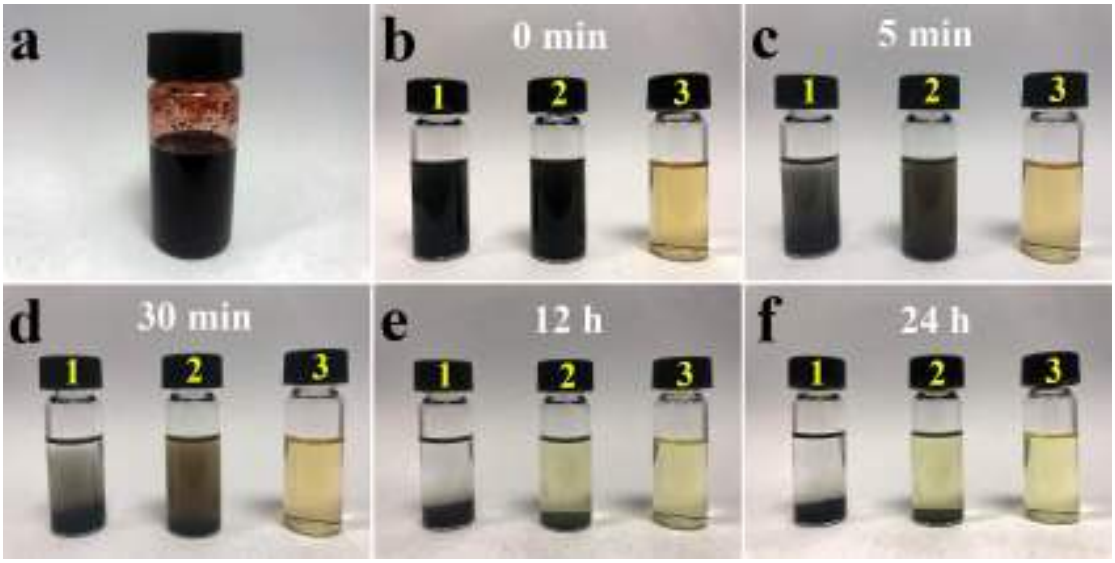

Fig. S23. Digital photos of (a) the as-prepared magnesium polysulfides, (b-f) process record of the interaction between sulfur host and magnesium polysulfides by adding Ti_3C_2@CoO (No.1) and Ti_3C_2-350 (No.2). No. 3 represents the magnesium polysulfides in diglyme solvent.

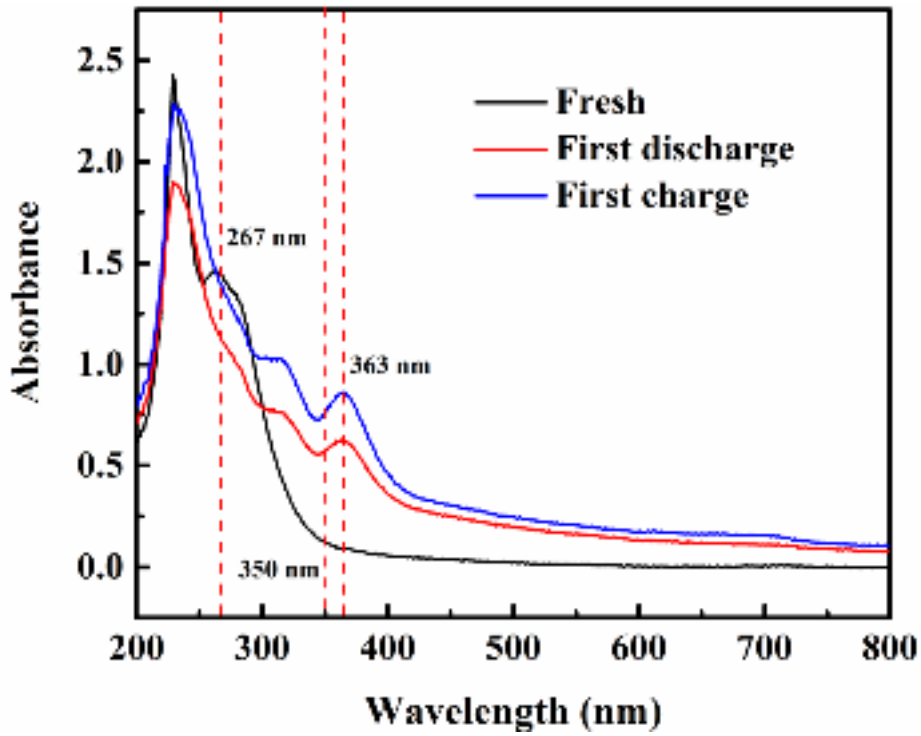

Fig. S24. UV-vis curves of electrolytes in different state: pristine, 1st discharge and 1st charge.

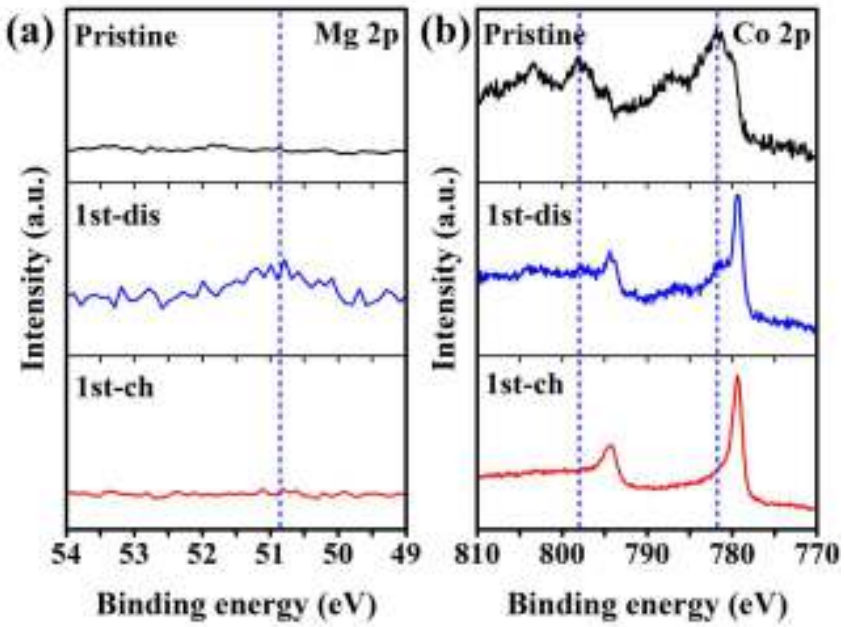

Fig. S25. High-resolution XPS analysis. Mg 2p and Co 2p of the S-Ti_3C_2@CoO cathode: pristine, 1st discharge and 1st charge.

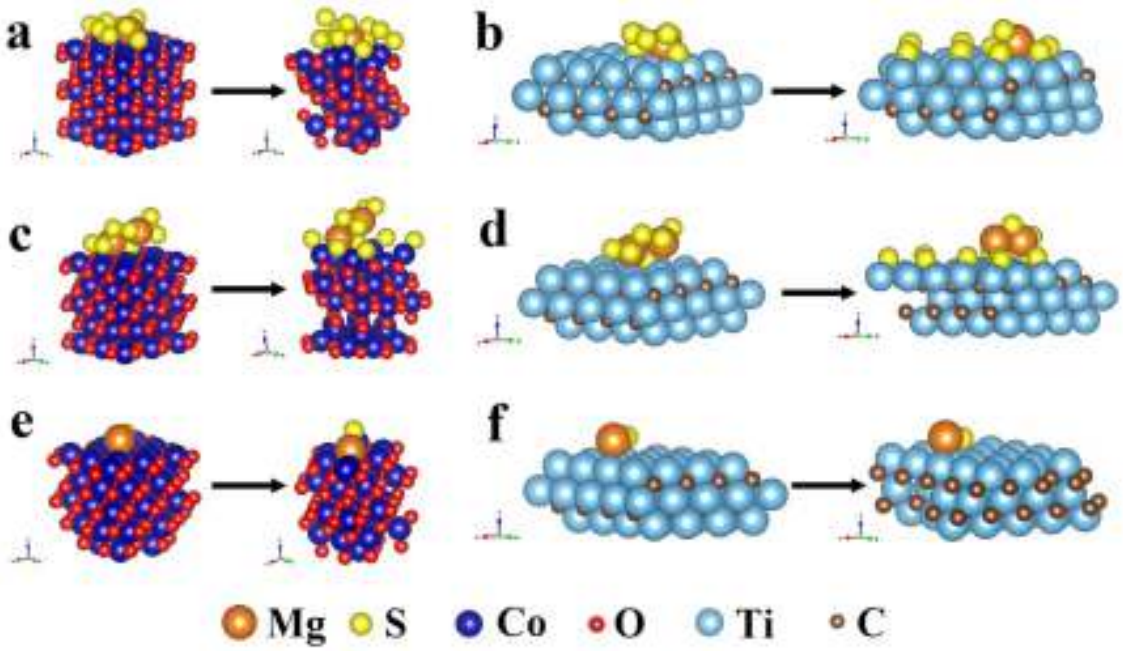

Fig. S26. DFT calculation (side view) of the adsorption models of (a) MgS_8, (c) MgS_4 and (e) MgS on the CoO (200) facet. DFT calculation of the adsorption models of (b) MgS_8, (d) MgS_4 and (f) MgS on the Ti_3C_2 (002) facet (Vienna Ab-Initio Simulation Package (VASP)).

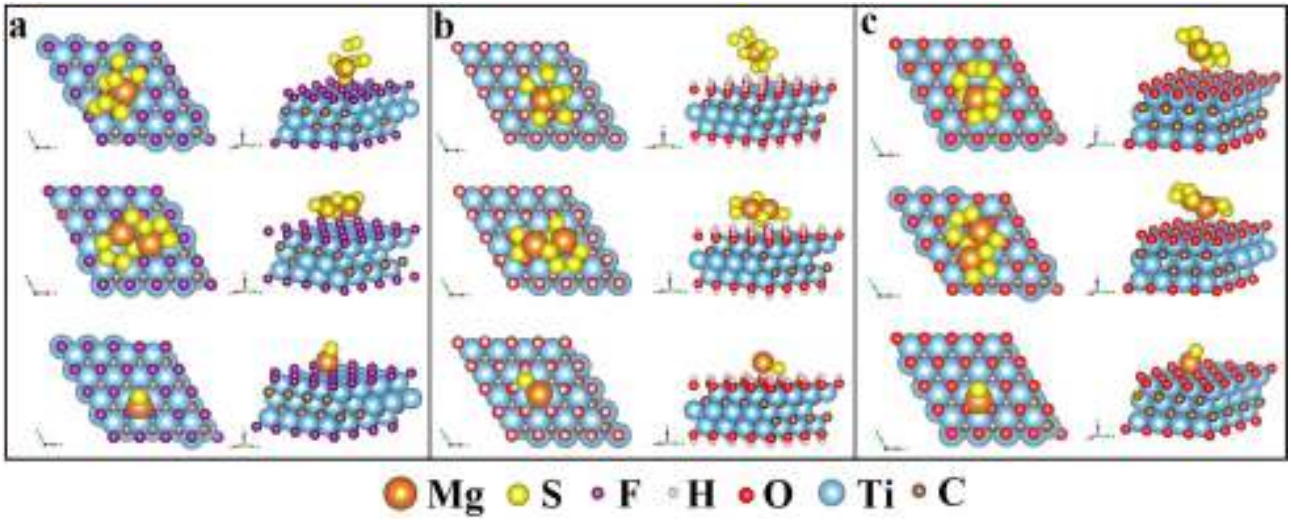

Fig. S27. DFT calculation of the adsorption models of MgS_8, MgS_4 and MgS on (002) on (002) planes of (a) $Ti_3C_2F_2$, (b) $Ti_3C_2(OH)_2$ and (c) $Ti_3C_2O_2$ from the front and side views.

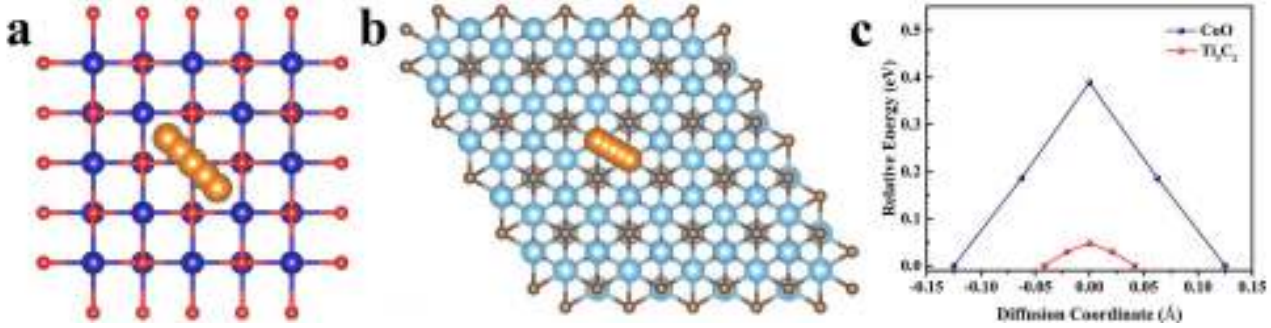

Fig. S28. Top view of the Mg ion diffusion pathways for (a) CoO and (b) Ti_3C_2. (c) Energy profiles for diffusion processes of Mg^{2+}on the CoO and Ti_3C_2, respectively.

Table S1 Comparison of electrochemical performance of magnesium sulfur batteries with previous reports. All batteries use electrolytes without Li salt additives.

Sulfur host materials	**Sulfur content (wt. %)**	**Electrolyte**	**Discharge plateau (V vs. Mg)**	**Current density (mA g^{-1})**	**Discharge capacity(mAh g^{-1})-(Cycle number)**	**Ref**
Carbon black	61	0.4 M HMDSMgCl/1.2M $AlCl_3$/THF	~ 0.9	~ 50	1200 (1) 394 (2)	[S1]
CMK-3	55	1.2 M $(HMDS)_2Mg$-(AlCl3)2-$MgCl_2$/PP14TFSI/diglyme	1.65	20	520(1) 150(20)	[S2]
CMK-3	55	1.2 M $(HMDS)_2Mg$-$(AlCl_3)_2$-$MgCl_2$/PP14TFSI/tetraglyme	1.6	20	600 (1) 250 (20)	[S2]
BUMB18C6	37.8	0.5 M $Mg(TFSA)_2$/triglyme	~0.5	16.8	608 (1) 23 (10)	[S3]
UOEE	47.3	0.7 M $Mg(TFSA)_2$/triglyme	~0.25	16.8	460(1) 68(10)	[S3]
N-doped graphene	50	0.3 M $MgCl_2$/0.6M $AlCl_3$/PYR14TFSI/THF	~ 0.75	16.8	700 (1) 130 (5) 70 (20)	[S4]
rGO	49	0.9 M $(HMDS)_2Mg$/$(AlCl_3)_2$/$MgCl_2$/tetraglyme	1.3-1.72,0.7-1.3	20	1024 (1) 296 (5) 219 (50)	[S5]
CNF	50	0.9 M $(HMDS)_2Mg$/$(AlCl_3)_2$/$MgCl_2$/tetraglyme	1-1.5	83	950(1) 1150(2) 700(20)	[S6]
ACC-507-20	1 mg cm^{-2}	1 M $Mg(TFSI)_2$/$MgCl_2$/DME	1.0-1.3	100	840 (1) 590 (110)	[S7]
CMK-3	55	0.4 M $Mg[B(hfip)_4]$/DME	168	1.25-1.5	800 (1) 200(100)	[S8]

ACC-507-20	0.8-1 mg cm^{-2}	0.5M $Mg(TFSI)_2/I_2$/DME	1.5	168	1200 (1) 550 (10)	[S9]
carbon black	80	0.5 M $(HMDS)_2Mg/(AlCl_3)_2$ /diglyme	0.9-1.2	83	710 (1) 420 (30)	[S10]
Ti_3C_2@CoO	59	1 M $Mg(TFSI)_2/(AlCl_3)_2$/ Diglyme	1-1.3	100	1500(1) 1060(5) 801(10) 540(70)	This work

Table S2. N_2 adsorption and desorption isotherms and pore size distribution of Ti_3C_2-350 and Ti_3C_2@CoO.

Sample	BET surface area (m^2 g^{-1})	BJH pore size(nm)
Ti_3C_2-350	57.2	4.3
Ti_3C_2@CoO	84.3	3.8

Table S3. EDX results of S-Ti_3C_2@CoO composites.

elements	wt. %
C	7.55
O	12.07
S	42.57
Ti	14.18
Co	23.63

Table S4. EDX results of S-(Ti_3C_2-350) composites.

elements	**wt. %**
C	13.63
O	3.88
F	6.18
S	41.38
Ti	34.93

Table S5. Calculated E_{ads} of MgS_8, MgS_4 and MgS on (002) plane of $Ti_3C_2T_x$ (T=F, OH and O)

$Ti_3C_2T_x$	MgS_8	MgS_4	MgS
$Ti_3C_2F_2$	1.49	-0.015	-0.0030
$Ti_3C_2(OH)_2$	1.46	-0.33	-0.17
$Ti_3C_2O_2$	0.0011	-0.0062	-0.063

References

[S1] H.S. Kim, T.S. Arthur, G.D. Allred, J. Zajicek, J.G. Newman, A.E. Rodnyansky, A.G. Oliver, W.C. Boggess, J. Muldoon, Nat. Commun. 2011, 2, 427.

[S2] Z. Zhao-Karger, X. Zhao, D. Wang, T. Diemant, R.J. Behm, M. Fichtner, Adv. Energy Mater. 2015, 5, 1401155.

[S3] K. Itaoka, I.-T. Kim, K. Yamabuki, N. Yoshimoto, H. Tsutsumi, J. Power Sources 2015, 297, 323.

[S4] W. Li, S. Cheng, J. Wang, Y. Qiu, Z. Zheng, H. Lin, S. Nanda, Q. Ma, Y. Xu, F. Ye, M. Liu, L. Zhou, Y. Zhang, Angew. Chem. Int. Ed. 2016, 55, 6406.

[S5] B.P. Vinayan, Z. Zhao-Karger, T. Diemant, V.S. Chakravadhanula, N.I. Schwarzburger, M.A. Cambaz, R.J. Behm, C. Kubel, M. Fichtner, Nanoscale 2016, 8, 3296.

[S6] X. Yu, A. Manthiram, ACS Energy Lett. 2016, 1, 431.

[S7] T. Gao, S. Hou, F. Wang, Z. Ma, X. Li, K. Xu, C. Wang, Angew. Chem. Int. Ed. 2017, 56, 13526.

[S8] Z. Zhao-Karger, M.E. Gil Bardaji, O. Fuhr, M. Fichtner, J. Mater. Chem. A 2017, 5, 10815.

[S9] X. Li, T. Gao, F. Han, Z. Ma, X. Fan, S. Hou, N. Eidson, W. Li, C. Wang, Adv. Energy Mater. 2018, 8, 1701728.

[S10] Y. Xu, W. Li, G. Zhou, Z. Pan, Y. Zhang, Energy Stor. Mater. 2018, 14, 253.